ICAS Paper No. 70–10

CONTROL OF TURBULENT BOUNDARY LAYERS BY UNIFORM INJECTION AND SUCTION OF FLUID

by
J. C. Rotta, Member of the Staff
DFVLR-Aerodynamische Versuchsanstalt
Göttingen, Germany

The Seventh Congress of the International Council of the Aeronautical Sciences

CONSIGLIO NAZIONALE DELLE RICERCHE, ROMA, ITALY / SEPTEMBER 14-18, 1970

Price: 400 Lire

CONTROL OF TURBULENT BOUNDARY LAYERS BY UNIFORM INJECTION AND SUCTION OF FLUID[+)]

J. C. Rotta

Deutsche Forschungs- und Versuchsanstalt
für Luft- und Raumfahrt
Aerodynamische Versuchsanstalt Göttingen

Abstract

Experimental and theoretical investigations on turbulent boundary layers with uniform injection and suction, having constant fluid properties, are carried out. Velocity profiles are measured at several stations along a flat porous plate. The law of the wall, including the viscous sublayer, is formulated. Adding Coles' law of the wake, an analytical presentation of the whole velocity profile is given, which forms the base of a procedure, to determine the skin friction coefficients from the experimental velocity profiles. The results are compared with the skin friction coefficients, obtained from surface Pitot tube measurements.

Equilibrium boundary layers are calculated, using alternatively Bradshaw's shear stress transport equation and A. M. O. Smith's eddy viscosity relation. Both methods yield almost equal results. The calculated and experimental skin friction coefficients agree well. The predicted shape factors are too low at high injection velocities and too high at high suction velocities.

Nomenclature

A	van Driest constant, Eq. (8)
B	wake factor, Eq. (10)
B_2	constant, Eq. (10)
C	constant of integration, Eq. (7)
c_f	local skin friction coefficient, $2\tau_W/(\varrho U_\infty^2)$
d	outer diameter of Pitot probe
f	dimensionless function, law of the wall, Eq. (6)
H_{12}	shape factor, δ_1/δ_2
H_{32}	shape factor, δ_3/δ_2
m	number of measurements of a traverse
p_P	dynamic pressure, i.e. difference between Pitot and static pressure
U, V	velocity components in x- and y-direction
$-\overline{uv}$	Reynolds shear stress
u_τ	shear stress velocity, $\sqrt{\tau_W/\varrho}$
v	deviation, $(U_m - U_c)/U_\infty$
w	wake function
w_2	additional velocity distribution, Eq. (11)
x, y	coordinates normal and parallel to the surface
y^*	dimensionless wall distance, yu_τ/ν
δ	total boundary layer thickness
δ_1	displacement thickness, $\int_0^\delta \left(1 - \frac{U}{U_\infty}\right) dy$
δ_2	momentum thickness, $\int_0^\delta \frac{U}{U_\infty}\left(1 - \frac{U}{U_\infty}\right) dy$
δ_3	kinetic energy thickness, $\int_0^\delta \frac{U}{U_\infty}\left[1 - \left(\frac{U}{U_\infty}\right)^2\right] dy$
ε	eddy viscosity, Eq. (23)
$\varkappa$	v. Kármán constant, Eq. (7)
ν	kinematic viscosity
ϱ	density
σ	root mean square deviation
τ	shear stress
Φ	calibration function, Eq. (19)

Subscripts

c	calculated value
m	measured value
W	wall conditions
∞	free stream conditions

1. Introduction

Turbulent boundary layer control by injection is an effective means to reduce the skin friction and heat transfer. In fact, the techniques of ablation and transpiration cooling, which are used for thermally protecting the surfaces of missiles and reentry vehicles from aerodynamic heating, are characterized by a mass transfer through the sur-

[+)] This work was sponsered by the Deutsche Forschungsgemeinschaft

face of the body. Turbulent boundary layer control by suction is applied, when boundary layer separation is to be prevented.

Many investigations are devoted to the simple case of constant fluid property boundary layers with uniform blowing or suction. A review of the previous work is found in Ref. 1. The main purpose of such work is to study the basic flow phenomena and the principles of computational methods, hoping that these may apply to more complex cases. These are also the objectives of the experimental and theoretical investigations, which are discussed in the present paper.

2. Experimental Investigation

2.1 Description of the Experiments

To begin with, a brief description of the experimental work shall be given. The tests have been carried out in the Low Turbulence Wind Tunnel of the AVA, which has a contraction ratio of 1:15. The test plate, consisting of a 4.5 mm thick porous polyethylene plate, 700 mm wide and 1 400 mm long, was built into the side wall of the wind tunnel. The pores were about 50 µ wide. The test surface was hydraulically smooth.

A sketch of the test arrangement is shown in Fig. 1. The plate was mounted on a steel grid,

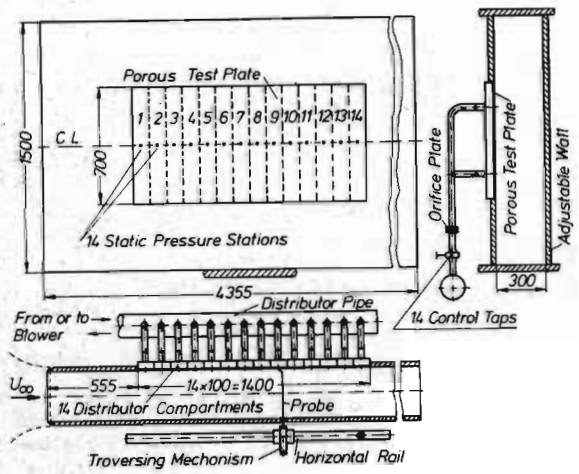

Fig. 1. Installation of the porous plate in the wind tunnel. All dimensions are in millimetres

which was closed from behind by an aluminium plate and served as a distributer box with 14 compartments. The injected air was supplied by a radial blower and had the same temperature as the free stream. For the tests with suction, the blower was reversed. The supply to each compartment could be regulated by a tap. The rate of mass flow was measured by an orifice plate. A uniform injection and suction distribution could be established despite of some irregularities in the permeability of the plate.

Fourteen static pressure stations, which consisted of short pieces of tubes inserted in the porous plate, were provided along the center line. The Pitot probe with an outer diameter of 0.28 mm at the tip was traversed through the adjustable wall opposite to the test plate.

Boundary layer profiles have been measured along the center line in the middle of each compartment, excepting the positions 6, 7 and 14, where the frame work of the wind tunnel did not allow to bring in the probe. Measurements were made at constant pressure along the plate for two values of the free stream velocity, namely $U_\infty \sim 20$ m/sec and $U_\infty \sim 30$ m/sec. The suction and injection velocities varied between $V_W = -0.10$ m/sec and $+0.13$ m/sec. Each traverse included about 60 measurements. The effective distance of the Pitot probe was assumed to be 0.04 mm greater than the distance of the probe center from the surface. Turbulence correction was ignored. A fully turbulent boundary layer of about 13 mm total thickness existed at the leading edge of the porous plate.

With the experiments reported in the literature, the porous plate spans one of the wind tunnel walls entirely. The boundary layers, growing on the other walls, and the corner flow usually prevent the flow from being fully two-dimensional. With the present tests, the porous plate spans only a part of the wind tunnel wall. It was hoped that the disturbing effects of the side walls are minimized in this way. At the last measuring station, the width of the porous plate was greater than 50 times the displacement thickness at the highest injection rate.

2.2 Experimental Results

The experimental data were reduced and analyzed so that the effects of injection and suction could be studied and compared with theoretical results.

The development of the momentum thickness, δ_2, in the direction of mean flow is shown on Fig. 2 as a typical example. This confirms the well-known fact that the boundary layer grows faster, when the injection velocity, V_W, is increased. The inverse effect occurs, when fluid is removed from the boundary layer. With the higher suction velocity, namely $V_W = -0.08$ m/sec and $V_W = -0.10$ m/sec, the momentum thickness of the boundary layer tends to assume a constant value towards the downstream end of the porous plate, thus the state of an asymptotic turbulent suction layer is almost established here.

A more instructive information on the development of the boundary layer is gained from Fig. 3. Here, the shape factor H_{12} is plotted versus the distance from the leading edge. With increasing

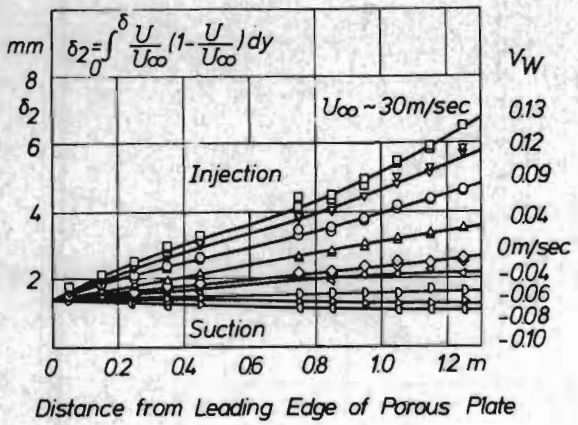

Fig. 2 Development of momentum thickness

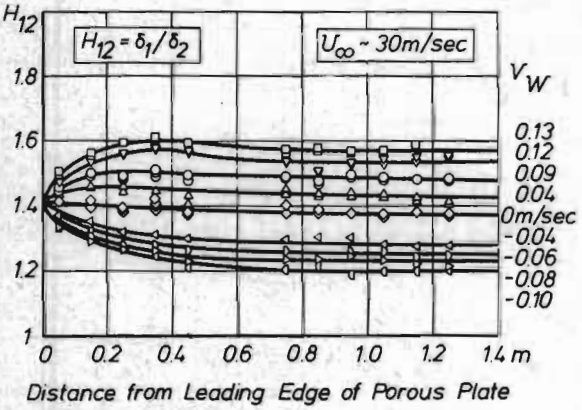

Fig. 3 Development of shape factor

injection velocity, the shape factor grows more rapidly at the foremost part of the porous plate and takes nearly constant values with the tendency to decrease slightly farther downstream. This means that the equilibrium state of a boundary layer with uniform injection and suction, respectively, is established downstream of the test station 8 ($x \geq 0.75$ m from leading edge). The slight decrease of H_{12} is caused by the growing boundary layer Reynolds number. Higher rates of injection produce more hollow velocity profiles, whereas suction gives fuller profiles.

An interesting feature comes to light, when the shape factor H_{32} is plotted versus H_{12}. All the data from measurements at different stations along the plate and with various injection and suction velocities, collapse on a narrow band, as is seen from Fig. 4. The relationship

$$H_{32} = \frac{4H_{12}}{3H_{12} - 1} \quad , \qquad (1)$$

which holds for power law profiles, namely

$$U/U_\infty = (y/\delta)^n \quad , \qquad (2)$$

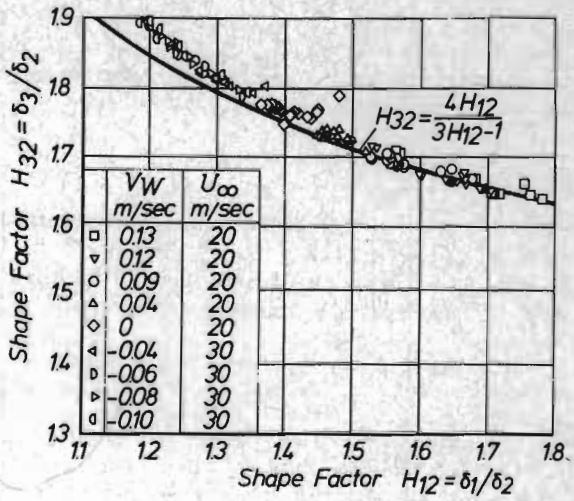

Fig. 4 Relationship between the shape factors

is shown as a solid curve. It is remarkable that for turbulent boundary layers on a porous plate and on impermeable surfaces almost the same relation exists between the two shape parameters. But it cannot be concluded from this observation that turbulent injection and suction profiles together with the profiles of boundary layers in variable pressure fields on impermeable walls form a one parametric family of curves.

Further details of the experimental results will be discussed in connection with the theoretical considerations.

3. The Flow Near the Wall

The treatment of the velocity distribution in proximity of the wall forms the core of the most of all theoretical work. In a layer, thin in comparison to the total boundary layer thickness, δ, the flow equations can be simplified by neglecting the derivatives of mean flow quantities with respect to x. Thus the equation of continuity gives, upon integration, a constant mean velocity normal to the surface,

$$V = V_W \quad . \qquad (3)$$

With this result, the integral of the boundary layer equation for the momentum in x-direction reads

$$\nu \frac{dU}{dy} - \overline{uv} = \frac{\tau_W}{\varrho} + V_W U \quad , \qquad (4)$$

which is the basic equation for mean momentum transport near the wall. The wall shear stress is given by

$$\frac{\tau_W}{\varrho} = \nu \left(\frac{dU}{dy}\right)_W \quad . \qquad (5)$$

The velocity, U, is a function of distance, y,

of the shear stress velocity, $u_\tau = (\tau_W/\varrho)^{1/2}$, the injection velocity, V_W, and the kinematic viscosity, ν. Dimensional analysis leads to

$$U = u_\tau f(y^*, V_W/u_\tau) \quad , \qquad (6)$$

where f is a function of the dimensionless distance y^* and the ratio V_W/u_τ. Eq. (6) is the extension of the universal law of the wall for turbulent flow over an impermeable surface.

The balance of kinetic fluctuation energy was discussed in Ref. 2. There is some indication that the diffusive and the convective energy transport in y-direction compensate each other in the fully turbulent layer. Thus the rates of turbulence production and viscous dissipation are locally in equilibrium. This provides some justification to apply the Prandtl mixing length relation with the mixing length $l = \varkappa y$. For large values of $y^*(\nu\, dU/dy << -\overline{uv})$, Eq. (4) has the solution

$$\frac{U}{u_\tau} = \frac{1}{\varkappa} \ln y^* + C + \frac{1}{4} \frac{V_W}{u_\tau} \left(\frac{1}{\varkappa} \ln y^* + C\right)^2 \quad , \qquad (7)$$

which has been derived by a number of authors. Actually, Eq. (7) is found in agreement with experiments, if a proper value is chosen for the integration constant, C.

To include the viscous sublayer, the theory is extended by introducing a damping function to the mixing length. With reference to van Driest's work, the Reynolds shear stress is approximated by

$$-\overline{uv} = (\varkappa y)^2 \left[1 - \exp\left\{-\frac{y\sqrt{u_\tau^2 + V_W U}}{(\nu A)}\right\}\right]^2 \left|\frac{dU}{dy}\right| \frac{dU}{dy} \quad . \qquad (8)$$

Substitution into Eq. (4) then yields

$$\frac{dU}{dy} = \frac{u_\tau^2}{\nu} \frac{df}{dy^*} = \frac{2(u_\tau^2 + V_W U)}{\nu + \sqrt{\nu^2 + 4\varkappa^2 y^2 \left[1 - \exp\left\{-\frac{y\sqrt{u_\tau^2 + V_W U}}{(\nu A)}\right\}\right]^2 (u_\tau^2 + V_W U)}} \quad . \qquad (9)$$

The velocity distribution and the integration constant C can be determined by integrating Eq. (9) numerically. A family of velocity distributions are plotted in a semi-logarithmic diagram on Fig. 5, showing the great influence of injection and suction velocity.

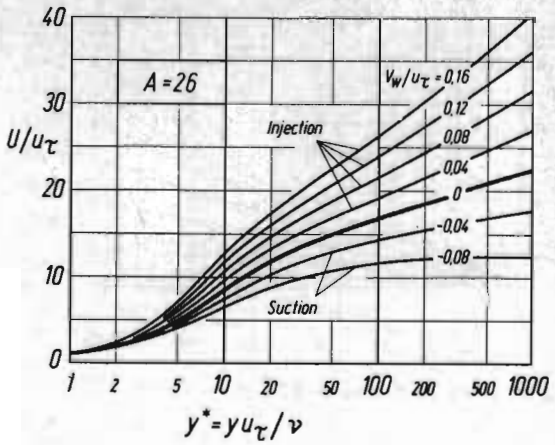

Fig. 5 Theoretical velocity distributions near the surface

The mechanism of turbulence and the intensities of the fluctuations are strongly affected by injection or suction. From Fig. 6 it is seen that the ratio of

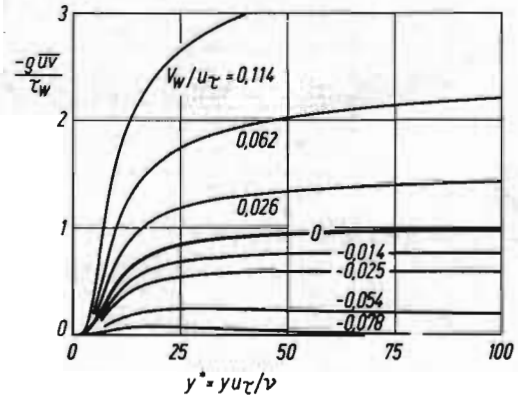

Fig. 6 Reynolds shear stress distributions near the surface

local Reynolds stress to wall shear stress varies in a wide range with V_W/u_τ. Another instructive quantity is the production of kinetic turbulent fluctuation energy, which equals to the work done on the Reynolds stress by the mean shear velocity. This term, $-\overline{uv}\, dU/dy$, can readily be calculated from the velocity distribution. Fig. 7 shows the kinetic energy production in a dimensionless form. The peak value increases enormously with injection velocity and decreases, when fluid is removed from the flow. In the light of these results, it can hardly be expected that the constant A has the same value for all injection and suction velocities. It was found from experiments that A decreases, when fluid is injected and increases, when fluid is sucked through the surface[2].

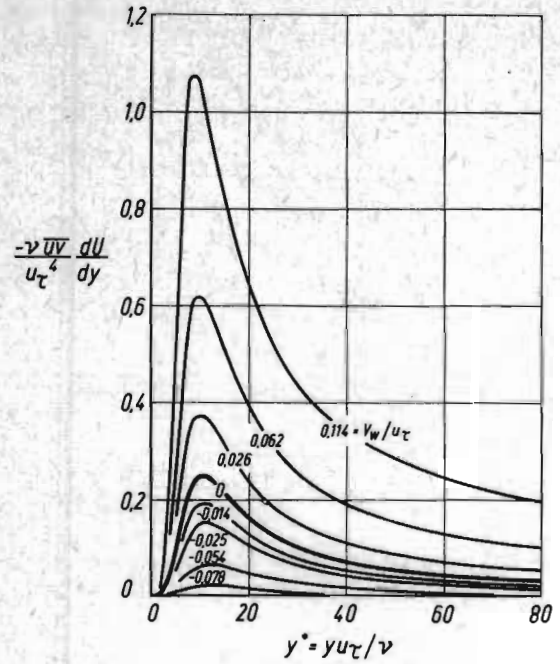

Fig. 7 Turbulent energy production in the viscous sublayer region

4. Determination of Skin Friction

The determination of the surface shear stress is one of the most important objectives of experimental research, in order to check and improve the calculation rules for the skin friction. Four different methods are known from the previous work.

1. Force measurements, using a skin friction balance.
2. Calculation from measured velocity profiles, using the momentum integral equation.
3. Determination from the dynamic pressure measured by a surface Pitot probe.
4. Determination from the measured pressure distribution near the surface.

All four methods have their own shortcomings. With the use of a friction balance, errors may arrise from the gaps of the floating element and the interruption of the uniform mass injection through the friction surface. A valuable contribution to overcome these difficulties has been made by H. Dershin, C.A. Leonard, and W.H. Gallaher[3].

Reliable results can hardly be expected at higher injection rates from the second method, since the shear stress appears as a small difference of two large terms, one of which has to be determined by differentiating the momentum thickness with respect to x. Even small deviations of the stream lines from being parallel falsify the results entirely.

The extension of the surface Pitot probe method to boundary layers on porous surfaces requires either a calibration of the probe on data obtained with another method, or some theoretical knowledge of the velocity distribution close to the wall[4]. Such a knowledge is also necessary, when the skin friction shall be determined from a measured velocity profile.

The methods 3 and 4 have been applied to the AVA measurements. In particular, a scheme was developed to determine the local skin friction coefficient and to extract additional information from the experiments, which may supplement the considerations of the preceding section.

4.1 Presentation of the Velocity Profiles

The basis of this scheme is the presentation of the entire velocity profile, which is constructed from the law of the wall and Coles' law of the wake[5]. An additional distribution is introduced in order to eliminate the abrupt change in the slope $\partial U/\partial y$ at the outer edge. Thus the following relation is used,

$$U = u_\tau\left[f(y^*,\ V_W/u_\tau) + \frac{B}{\varkappa}\, w(y/\delta) + \frac{B_2}{\varkappa}\, w_2(y/\delta)\right]. \quad (10)$$

Here f is calculated from Eq. (9) and depends on the constants $\varkappa$ and A. $w(y/\delta)$ is the Coles wake function, having the value $w(0) = 0$ and $w(1) = 2$. The distribution $w_2(y/\delta)$ is given by

$$w_2(y/\delta) = (y/\delta)^5(1 - y/\delta)(4y/\delta - 3) \quad . \quad (11)$$

The constant B_2 follows from the condition

$$y = \delta: \quad \frac{\partial U}{\partial y} = u_\tau\left[\frac{df}{dy^*}\,\frac{u_\tau}{\nu} - \frac{B_2}{\varkappa}\,\frac{1}{\delta}\right] = 0 \quad . \quad (12)$$

The local skin friction law is obtained from Eq. (10) putting $y = o$,

$$\sqrt{\frac{2}{c_f}} = \frac{U_\infty}{u_\tau} = f(\delta u_\tau/\nu,\ V_W/u_\tau) + 2\,\frac{B}{\varkappa} \quad . \quad (13)$$

This equation determines c_f, if the constants $\varkappa$, A, B are known and the local flow parameter, U_∞, V_W, δ, and ν are given. Since the velocity profile is specified by Eq. (10), the thickness parameters δ_1, δ_2 can also be calculated. Consequently, letting B assume arbitrary values, Eqs. (10) and (13) imply the local skin friction law in the form

$$c_f = F(Re_2,\ H_{12},\ V_W/U_\infty) \quad , \quad (14)$$

where $Re_2 = U_\infty\delta_2/\nu$. Eq. (14) is an extension of

the local friction law of turbulent boundary layers on impermeable surfaces. The presentation is more complex, of course, since three independent parameters are involved. However, this point shall not be treated here further.

4.2 Statistical Analysis of Experimental Velocity Profiles

We turn to the problem of using Eqs. (10) and (13) in conjunction with the measurements of velocity profiles. Given the values U_∞, V_W, ν, $\varkappa$, and A, Eq. (13) determines any one of the three parameters u_τ, δ, and B, if the other two are known. Consequently, velocity measurements at two different distances y are required, to determine all the three parameters. Any two pairs of values U, y of the traverse provide a set of values u_τ, δ, B, but each set probably differs from the other. This matter of fact suggests to attack the problem with methods of mathematical statistics, whereby all the values of a traverse are taken into account.

It is supposed that Eq. (10) provides an adequate approximation to the real velocity profile, and that the deviations of the measurements from this profile are random errors, being normally distributed. Then the principle of maximum likelihood requires that the root mean square deviation of the experimental data becomes a minimum. Actually, we went a step further and considered the van Driest constant, A, too as an unknown. An iterative procedure was applied so solve the nonlinear problem of finding the most probable values of u_τ, δ, A, and B. The von Kármán constant was assumed $\varkappa = 0.4$.

On Fig. 8 some profiles with different injection velocities are compared with the profiles calculated from Eq. (10). The same profiles are shown in a semilogarithmic diagram, in which the region close to the wall is stretched, Fig. 9. The visual exami-

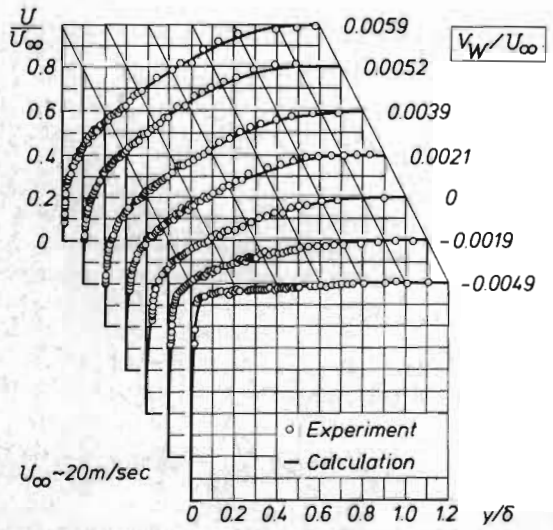

Fig. 8 Velocity profiles, on the porous plate, station 12

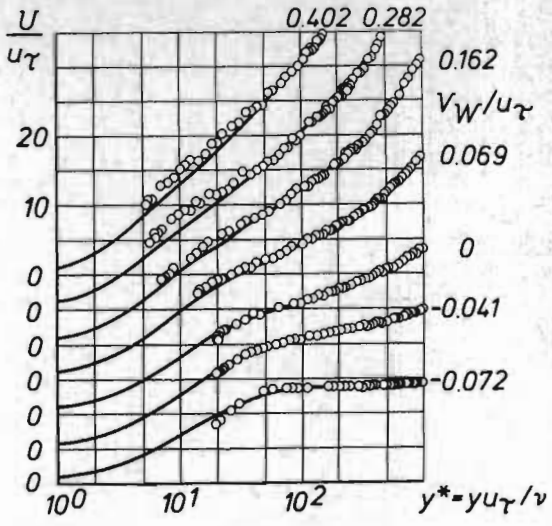

Fig. 9 Velocity profiles on the porous plate, station 12. Semilogarithmic diagram

nation of both Figures confirms that Eq. (10) provides really an adequate presentation of the velocity profiles. Moreover, the kind of treatment offers the possibility to apply wellknown test methods of mathematical statistics to check, whether or not there are significant deviations of the measurements from the profiles of Eq. (10). Just a few typical figures may be given for illustration.

The root mean square deviation, as defined by

$$\sigma = \left[\frac{1}{m-3}\sum^{m} v^2\right]^{1/2} \qquad (15)$$

is of the order of 1 p.c., where v is the deviation of an individually measured velocity, U_m, from the corresponding calculated value, U_c, and m is the number of measurements of a traverse. The mean error

$$\bar{v} = \frac{1}{m-2}\sum^{m} v \quad , \qquad (16)$$

is, on an average, one order of magnitude smaller than σ and has positive as well as negative values. In addition, we have calculated the correlation coefficient

$$k = \frac{\sum^{m}\left[(v-\bar{v})(y-\bar{y})\right]}{\left\{\sum^{m}(v-\bar{v})^2 \sum^{m}(y-\bar{y})^2\right\}^{1/2}} \quad , \qquad (17)$$

where $\bar{y} = \left(\sum^{m} y\right)/m$. The magnitudes of this correlation coefficient are, in most cases, below 10 p.c., and there are again positive and negative values. So far, there is no indication of systematic deviations.

The development of the local skin friction coeffi-

cient along the plate at different injection velocities is seen from Fig. 10. This diagram shows the

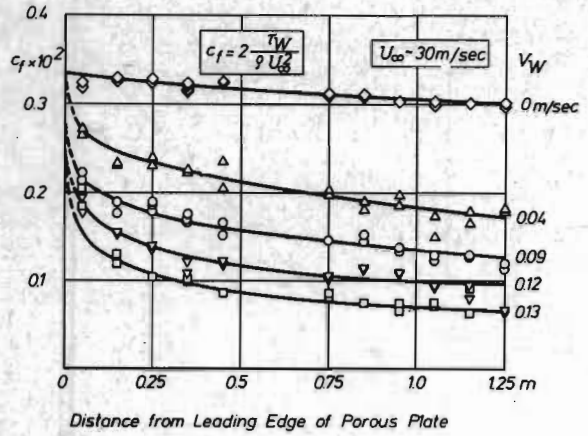

Fig. 10 Local skin friction coefficients on the porous plate with injection

familar decrease of c_f with growing V_W. In addition, it follows that c_f tends to change more rapidly towards the equilibrium values than the shape factor H_{12}. Fig. 11 presents local skin friction coefficients, when fluid is sucked away. This causes a substantial increase in c_f.

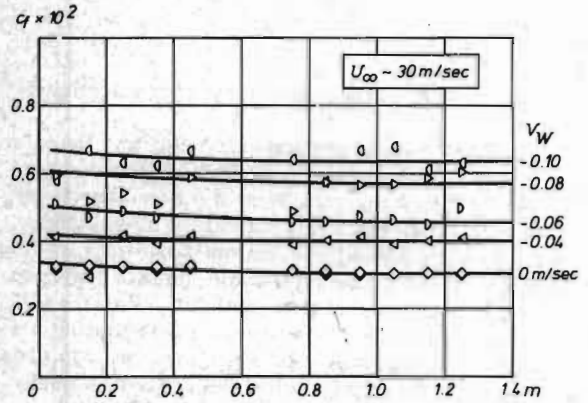

Fig. 11 Local skin friction coefficients on the porous plate with suction

Clearly, the values of u_τ (or c_f), δ, and A, determined by the described procedure, are statistical mean values, thus there exist a root mean square deviation for each value and covariances between different values. These quantities can be calculated, and statistical test methods can be used again to check the limits of confidence. The root mean square deviation of δ is generally very small (only a few per cent of δ), whereas the root mean square deviation of c_f amounts to 10 to 15 per cent of c_f for the injection cases and is very low for the suction profiles. The root mean square deviations of A are perceptibly higher. The values of c_f and A are determined mainly by the velocity measurements at smaller distances y, whereas measurements at larger y are responsible for δ. Consequently, c_f and A are statistically independent of δ. There is a strong correlation, however, between c_f and A. Actually, the value of A can be determined with moderate accuracy only.

According to the similarity conception of the law of the wall, A is a function of V_W/u_τ. Therefore, A is plotted versus V_W/u_τ in Fig. 12. This investigation includes more than 200

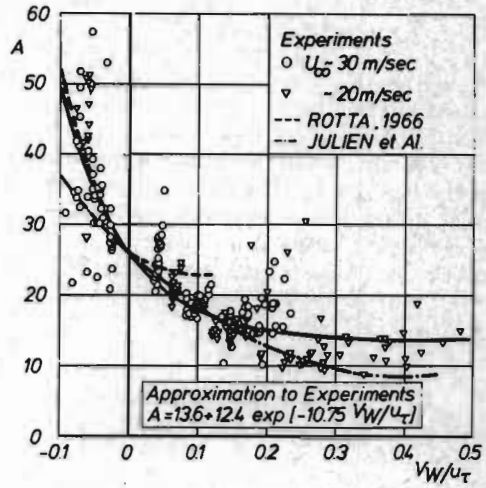

Fig. 12 Variation of the van Driest constant with injection velocity ratio

profiles. Despite the large scattering of the data points, the tendency of A, to decrease with growing V_W/u_τ, is clearly detectable. The relation

$$A = 13.6 + 12.4 \exp(-10.75\, V_W/u_\tau) \qquad (18)$$

is suggested as an approximation to the data. The previous estimation (Ref. 2), which was based on measurements of injection boundary layers by H.S. Mickley and R.S. Davis[6], and of suction boundary layers by A. Favre et al.[7], is shown as a dotted line. Also indicated is the result of H.L. Julien, W.M. Kays and R.J. Moffat[8].

The present results are in agreement with Julien's relation for the injection profiles ($V_W/u_\tau \leq 0.2$), and with the results of Ref. 2 for the suction profiles. A more exact answer with respect to the variation of A as a function of V_W/u_τ can be obtained not until reliable measurements deep in the viscous sublayer regime become available.

4.3 Surface Pitot Probe

As an alternative way to determine the skin friction, the surface Pitot tube method was studied.

The basis of this method is the universal law of the wall, according to which the surface shear stress can be related to the dynamic pressure, p_P, measured from a Pitot tube resting on the surface. For incompressible turbulent boundary layers on smooth, inpermeable surfaces, there exists the universal relation

$$\frac{p_P d^2}{4\varrho\nu^2} = \Phi\left(\frac{\tau_W d^2}{4\varrho\nu^2}\right) \quad . \qquad (19)$$

Thus τ_W can be determined, once the calibration function Φ is established.

The extension of Eq. (19) to flows with injection or suction results from a dimensional analysis, but the problem is to determine quantitatively the calibration function, which depends on the additional parameter $V_W d/\nu$. The dynamic pressure, p_P, indicated by the probe, corresponds approximately (but not exactly) to the velocity at the center of the probe. On the basis of this supposition, the following relation is proposed,

$$\frac{p_P d^2}{4\varrho\nu^2} = \left[\frac{f(y_d^*,\ V_W/u_\tau)}{f(y_d^*,\ 0)}\right]^2 \Phi\left(\frac{\tau_W d^2}{4\varrho\nu^2}\right) \quad . \qquad (20)$$

Thus the calibration function is calculated from the known calibration function for impermeable surfaces, Φ, and the law of the wall, Eq. (9), putting $y_d^* = u_\tau d/(2\nu)$. Eq. (20) has been used to calculate the skin friction coefficient from the measurement. The dynamic pressure was taken from the boundary layer traverses, while the probe was in contact with the surface. The calibration function, Φ, was given by Patel's work[9] and A was assumed constant. A comparison of these results with the skin friction data, obtained from the whole velocity profile, is presented for injection profiles on Fig. 13

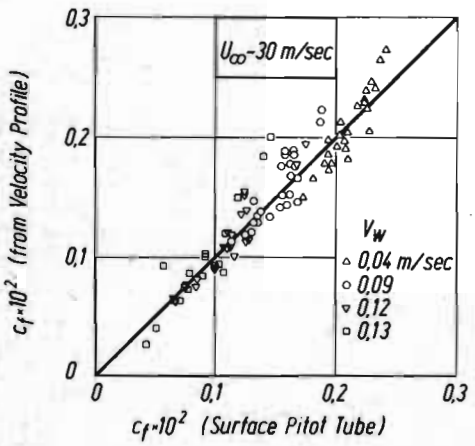

Fig. 13 Comparison of skin friction coefficients, injection. Symbols as on Figure 10

and for suction profiles on Fig. 14. On an average, the data from the two methods agree well with each other.

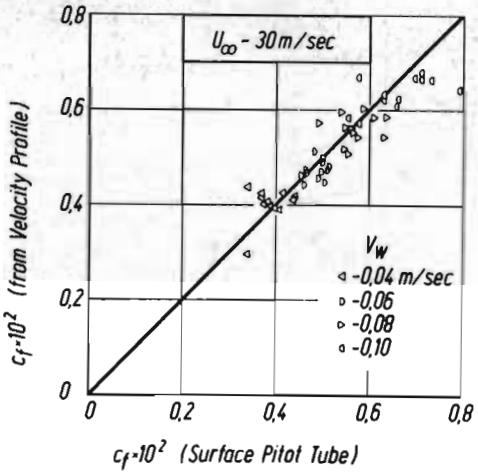

Fig. 14 Comparison of local skin friction coefficients, suction. Symbols as on Fig. 11

The surface Pitot tube method offers the advantage, to determine the skin friction from a single measurement. However, the results from the statistical method are considered to have greater accuracy.

5. Calculation of Boundary Layer Development

The final goal of any experimental and theoretical research is to create calculation methods for predicting the characteristics of a boundary layer, which will develop under arbitrarily given conditions. Most of the calculation methods for turbulent boundary layers on impermeable surfaces belong to the group of the integral methods. With these methods the problem is reduced to calculating a few global parameters like δ_2, δ_1 and c_f. In order to extend the empirical relations, on which such methods rest, to more complicated situations, a hudge volume of measurements is needed. Field methods, which are based on partial differential equations, appear to be more promising, although greater computational efforts are required.

Tentatively, calculations have been performed, using two known methods to treat the Reynolds shear stress. In the first case, Bradshaws's shear stress transport equation,

$$\frac{1}{2a_1\varrho}\left(U\frac{\partial\tau}{\partial x} + V\frac{\partial\tau}{\partial y}\right) =$$

$$= \frac{\tau}{\varrho}\frac{\partial U}{\partial y} - \frac{(\tau/\varrho)^{3/2}}{L} - \frac{\partial}{\partial y}\left[\frac{\tau}{\varrho}\left(\frac{\tau_{max}}{\varrho}\right)^{1/2} G\right] \quad , \qquad (21)$$

is used with the empirical functions,

$$\left.\begin{aligned} a_1 &= 0.15 \quad , \\ L &= \delta f_1(y/\delta) \quad , \\ G &= \left(\frac{\tau_{max}}{\varrho U_\infty^2}\right)^{1/2} f_2(y/\delta) \quad , \end{aligned}\right\} \quad (22)$$

given by P. Bradshaw, D.H. Ferriss, and N.P. Atwell[10]. τ_{max} denotes the maximum value of the shear stress.

Alternatively, the Boussinesq eddy viscosity relation,

$$\frac{\tau}{\varrho} = \varepsilon \frac{\partial U}{\partial y} \quad , \quad (23)$$

was applied with reference to the particular form of ε suggested by T. Cebeci and A.M.O. Smith[11]. A justification to use this relation is given by R.L. Simpson[12], who found ε to be substantially independent of blowing and moderate suction. In the inner region, the mixing length formula, according to Eq. (8), was used. In the outer region, the constant value of the eddy viscosity was multiplied by the intermittency factor,

$$\varepsilon = 0.0168\, U_\infty \delta_1 \gamma \quad , \quad (24)$$

where the intermittency factor is approximated by

$$\gamma = \left[1 + 5.5 \left(\frac{y}{\delta}\right)^6\right]^{-1} \quad . \quad (25)$$

The numerical solution of the partial differential equations,

$$\text{continuity:} \quad \frac{\partial U}{\partial x} + \frac{\partial V}{\partial y} = 0 \quad , \quad (26)$$

$$\text{momentum:} \quad U \frac{\partial U}{\partial x} + V \frac{\partial U}{\partial y} = \frac{1}{\varrho} \frac{\partial \tau}{\partial y} \quad , \quad (27)$$

was based on the assumption of equilibrium layers, having selfsimilar profiles (the variation of the Reynolds number is locally neglected). In other words, the following statements were used:

$$U = U_\infty \varphi(y/\delta), \quad V = U_\infty \psi(y/\delta), \quad \tau = \varrho U_\infty^2 g(y/\delta), \quad (28)$$

where φ, ψ, and g are dimensionless functions of y/δ. A Ritz-Galerkin type of method was applied. The velocity profile was approximated by Eq. (10) with three additional distribution functions, satisfying the boundary condition at the surface and at $y = \delta$. The differential equations were fulfilled at four collocation points, equally distributed across the layer thickness.

The skin friction coefficients, calculated from Bradshaw's relation, are compared with experimental data of stations 8 - 13 on Fig. 15. The

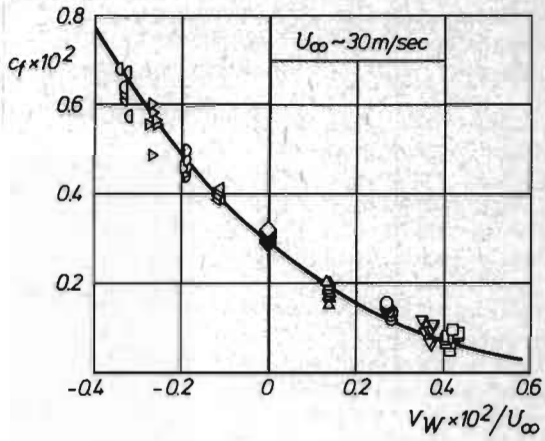

Fig. 15 Local skin friction coefficient of equilibrium boundary layer. Experiments at stations 8 - 13
——— theory, $U_\infty \delta/\nu = 5 \times 10^4$

Reynolds number of the calculation is $U_\infty \delta/\nu = 5 \times 10^4$. The agreement is good. The calculated shape factor H_{12} agrees less good with the experiments, Fig. 16. Nevertheless, the theory predicts the tendency of H_{12}, to increase with injection velocity.

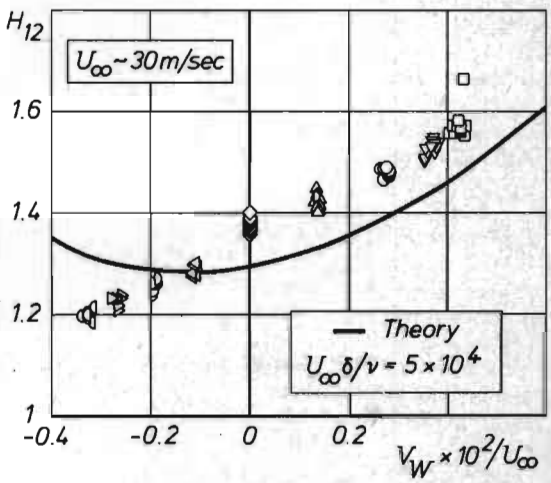

Fig. 16 Shape factor of equilibrium boundary layer. Experiments at station 8 - 13

A surprising finding is that the eddy viscosity concept yields nearly the same results as Bradshaw's relation. In fact, the differences of the two methods are hardly discernible on diagrams like Figs. 15 and 16.

6. Concluding Remarks

Velocity profile measurements on a porous flat plate show that equilibrium boundary layers with injection are established at a downstream distance of about 50 times the total boundary layer thickness at the leading edge of the porous plate. Asymptotic suction layers are accomplished at a suction velocity ratio $V_w/U_\infty = -0.003$.

The law of the wall, combined with Coles' wake function, provides a good analytical approximation to the velocity profiles. Local skin friction coefficients, determined from these velocity profiles and from the surface Pitot tube method agree, on the average, with each other.

Exploratory calculations of equilibrium boundary layers, based on Bradshaw's shear stress transport equation and on A.M.O. Smith's eddy viscosity relation, respectively, yield nearly identical results. The calculated skin friction is found in good agreement with the experiments. The variation of the shape factor with injection velocity is underestimated by the theory.

References

1. Simpson, R.L., Moffat, R.J., and Kays, W.M., "The Turbulent Boundary Layer on a Porous Plate: Experimental Skin Friction with Variable Injection and Suction", Int. J. Heat Mass Transfer, Vol. 12, 1969, pp. 771-789

2. Rotta, J.C., "Ueber die Geschwindigkeitsverteilung bei turbulenter Strömung in der Nähe poröser Wände", DLR FB 66-45, 1966

3. Dershin, H., Leonard, C.A., and Gallaher, W.H., "Direct Measurements of Skin Friction on a Porous Flat Plate with Mass Injection", AIAA Journal, Vol. 5, No. 11, November 1967, pp. 1934-1939

4. Simpson, R.L., and Whitten, D.G., "Preston Tubes in the Transpired Turbulent Boundary Layer", AIAA Journal, Vol. 6, No. 9, September 1968, pp. 1776-1777

5. Coles, D., "The Law of the Wake in the Turbulent Boundary Layer", J. Fluid Mech., Vol. 1, 1956, pp. 191-226

6. Mickley, H.S., and Davis, R.S., "Momentum Transfer for Flow over a Flat Plate with Blowing", NACA TN 4017, 1957

7. Favre, A., Dumas, R., Verollet, E., and Coantic, M., "Couche limite turbulente sur paroi poreuse avec aspiration", Journal de Mécanique, Vol. 5, No. 1, Mars 1966, pp. 1-28

8. Julien, H.L., Kays, W.M., and Moffat, R.J., "The Turbulent Boundary Layer on a Porous Plate: Experimental Study of the Effects of a Favorable Pressure Gradient", Rep. No. HMT-4, Thermosciences Division, Stanford University, California, April 1969

9. Patel, V.C., "Calibration of the Preston Tube and Limitations on its Use in Pressure Gradients", J. Fluid Mech., Vol. 23, 1965, pp. 185-208

10. Bradshaw, P., Ferriss, D.H., and Atwell, N.P., "Calculation of Boundary Layer Development Using the Turbulent Energy Equation", J. Fluid Mech., Vol. 28, 1967, pp. 593-616

11. Cebeci, T., and Smith, A.M.O., "A Finite-Difference Solution of the Incompressible Turbulent Boundary Layer Equations by an Eddy Viscosity Concept", Proc. Computation of Turbulent Boundary Layers - 1968 AFOSR-IFP-Stanford Conference, S.J. Kline, M.V. Morkovin, G. Sovran, D.J. Cockrell (Eds.), Vol. 1, 1969, pp. 346-355

12. Simpson, R.L., "Characteristics of Turbulent Boundary Layers at Low Reynolds Numbers with and without Transpiration", to be published